JOURNAL OF MATERIALS SCIENCE 24 (1989) 2801–2807

Relationships between rare earth oxide polymorphs in thin films treated with water vapour

M. GASGNIER, G. SCHIFFMACHER, P. CARO
ER210, C.N.R.S. Bellevue, 1 place Aristide Briand, 92195 Meudon Cedex, France

The limits (temperature–pressure) of the phase transitions of the different rare earth oxide (as R_2O_3 and RO_2) compounds are still the subject of a large amount of discussion. In the case of thin films, these phenomena are increased overall, when such materials are irradiated by an electron beam or when they are widely contaminated by water vapour. For praseodymium and neodymium the formation of stable B-Pr_2O_3 and B-Nd_2O_3 crystals throughout an A-R_2O_3 matrix and, in like manner, the epitaxy of the B-Tb_2O_3 and TbO_2 phases, appear as very unexpected phenomena. These facts are tentatively explained as a consequence of acoustic elastic wave (as shock-waves) generation which could be compared to high-pressure phenomena.

1. Introduction

The phase diagrams of R_2O_3 polymorphic oxides (R = rare earth) were established as a function of temperature from pure materials [1, 2]. Classically, in the bulk, the R_2O_3 series is characterized by the C-form (cubic centred) for all the elements, including scandium and yttrium, the B-form (monoclinic) for rare earths from promethium to holmium, and the A-form (hexagonal) for light rare earths from lanthanum to neodymium, whereas the RO_x (or R_nO_{2n-2}) series (R = cerium, praseodymium and terbium) is defined, between $x = 1.5$ and $x = 2$ (or $n = 4$ and $n = \infty$), by a great number of structures (hexagonal, monoclinic and triclinic) built on the fluorite-like lattice of the RO_2 compound. In the case of thin films and thin flakes the formation of the B-Pr_2O_3 and B-Nd_2O_3 structures and unexpected RO_x phases, was observed by electron microscopy [3–12]. From all these experiments two crystal problems emerge: the formation of the B-form for light elements (praseodymium and neodymium) and the formation of the RO_x known and unknown structures. The first seems linked to special pressure–temperature conditions and, from evidence, to the stability of the B-structure. The second is due to the unknown oxygen-vacancy rearrangement mechanism throughout the fluorite lattice. As reported in recent papers [13, 14], new experiments have allowed these problems to be approached in the framework of a new procedure. It was proved that water vapour can be a prominent parameter (as a catalytic impurity) to induce intricate phase transformation phenomena, the latter being widely amplified by the electron-beam irradiation inside an electron microscope. Different papers were devoted to the interaction of Nd_2O_3 and Pr_2O_3 compounds with water [15–18], but only Shafer and Roy [15] report the formation of the B-Nd_2O_3 structure in the course of high hydrothermal pressure and Goldschmidt *et al.* [16] observed this phase after rapid heating of $Nd(OH)_3$ at 1600 K. These results were never reproduced, peculiarly by Warshaw and Roy [17] and Roth and Schneider [18] which speculated upon the existence of B-Ce_2O_3 and B-Pr_2O_3. Now, more recent experiments have proved the role of water in relation to the physico-chemical properties of the sesquioxides. Palatnik *et al.* [19] report that the B $\leftrightarrow$ C reversibility, observed with Eu_2O_3 thin films, is strongly dependent on the presence of water molecules. These, as detected by infrared measurements, are localized in the vacant sites of the C-Eu_2O_3 sub-lattice. Norby and Kofstad [20] have shown the wide change of resistivity, for Y_2O_3 powders, as a function of the water vapour partial pressure and of temperature.

The aim of this paper is to show that, initially, metallic thin films (praseodymium (Pr), neodymium (Nd) and terbium (Tb)), strongly contaminated with water vapour, can crystallize according to stable or metastable well-defined oxides, but epitaxially linked to the basic A-(Pr_2O_3, Nd_2O_3) or C- or B-Tb_2O_3 stable structures.

2. Experimental methods

Experimental details were reported in previous papers [13, 14]. Concisely, the films are detached from NaCl substrates by floating off in distilled water and then picking up on copper grids. Then they are deliberately exposed to water vapour, in air, for 2 or 3 h. Lastly they are put inside a conventional transmission electron microscope (Jeol 100 C, 100 kV) and heated using the electron beam after removal of the condenser aperture. This permits annealing of a very small area (1 to 2 μm^2) of the sample up to a temperature close to 2000 K [21]. As a function of the annealing mode (progressive or pulse-annealing) and of the focusing,

0022–2461/89 $03.00 + .12 © *1989 Chapman and Hall Ltd.*

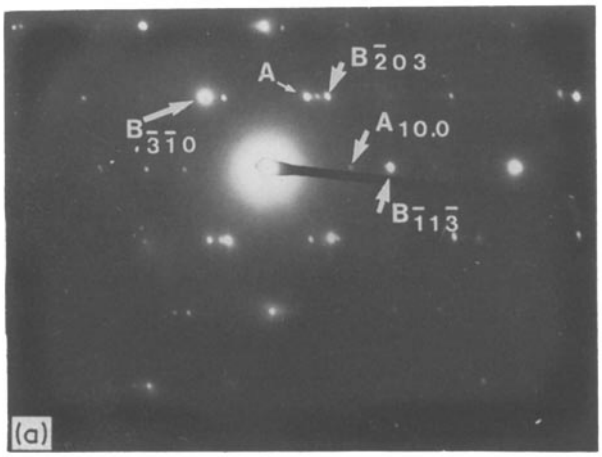

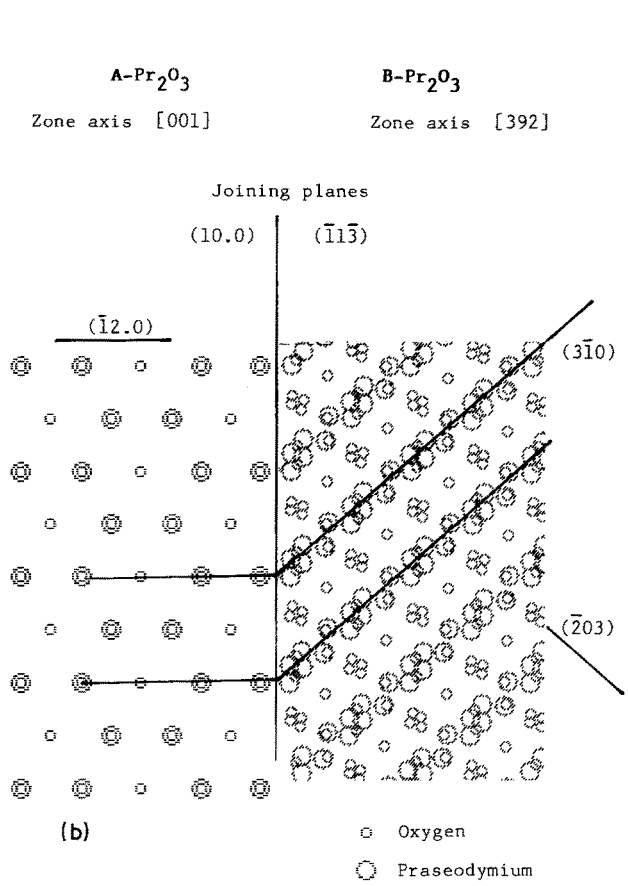

Figure 1 Well-defined epitaxial correlation between two A- and B-Pr_2O_3 crystals. (a) Electron diffraction pattern. (b) Drawing of the projection of the two lattices put side by side to illustrate the epitaxy.

the crystallization phenomena occur either at the beam impact area or in a close surface around it inducing a temperature gradient effect.

Epitaxial correlation of the different structures observed during thin film annealing, was drawn up in terms of the projection of the lattices, by means of a microcomputer. Firstly the program generates the position of all the atoms of the cell according to the (x), (y) and (z) values of their Wyckoff position and of the symmetries of their space group. Then, by adequate rotations, the direction of the projection is taken as the c-axis and a new two-dimensional cell is calculated. The basic two-dimensional cell, or its multiples obtained by translations along x- and y-axes, is the projection of the atomic positions along the z-axis. It is displayed on the computer screen and then printed. The trace of the indexed atomic planes, perpendicular to the projection plane, can be drawn in order to orientate the projected cell. The drawing of projections are, then, put side by side to determine the fit between both atomic arrays.

3. Unexpected epitaxies in rare earth oxide thin crystals

During annealing of praseodymium, neodymium and terbium metallic thin films, numerous phenomena occur [21]. The crystalline growth mechanism and the chemical transitions are often intricate and correlated to the intensity of the electron-beam irradiation. As demonstrated previously, structural information was often difficult to resolve. The corresponding electron diffraction patterns (EDP) were therefore very complex due to the coexistence (or to the superposition) of several diffraction spots from different structures. This is the case for some peculiar epitaxial situations described in this paper.

3.1. Praseodymium oxides

3.1.1. A → B epitaxy

EDP such as those of Figs 1a and 2a show the simultaneous presence of A- and B-Pr_2O_3 with epitaxial relationships. In the first case (Fig. 1b) the zone axes are, respectively, $\langle 0\,0\,1\rangle$ and $\langle 3\,9\,2\rangle$ for the A- and B-Pr_2O_3 structures. The joining planes are $(1\,0\,.\,0)_A$ and $(\bar{1}\,1\,\bar{3})_B$. The connected planes are $(\bar{1}\,2\,.\,0)_A$ and $(3\,\bar{1}\,0)_B$. These are not parallel, the angle between $(3\,\bar{1}\,0)_B$ and $(\bar{1}\,1\,\bar{3})_B$ being equal to 49.35°. However, as the $(3\,\bar{1}\,0)$ atomic planes ($d_{3\bar{1}0} = 0.290$ nm) intersect the $(\bar{1}\,1\,\bar{3})$ plane with a periodicity equal to 0.382 nm, and as for the hexagonal structure the two-fold value of the interplanar distance of the $(\bar{1}\,2\,.\,0)$ plane is equal to 0.383 nm, the fit is nearly perfect ($\approx 1\%$). This epitaxial situation is the more frequently observed. This can also be explained by the fact that the $\langle 3\,9\,2\rangle_B$ projection is characterized by dense atomic planes.

In the second case (Fig. 2b) the zone axis is $\langle 0\,0\,1\rangle$ for the A-structure and $\langle 0\,0\,1\rangle$ for the B-structure. The joining planes are $(1\,0\,.\,0)_A$ and $(1\,0\,0)_B$. The structure projections along the zone axes can be drawn with the $(\bar{1}\,2\,.\,0)_A$ plane parallel to the $(0\,1\,0)_B$ plane, which leads to the possible epitaxial relation:

$$d_{(1\,2\,.\,0)_A} = 0.193\,\text{nm}$$

$$d_{(0\,2\,0)_B} = 0.186\,\text{nm}$$

with a ratio divergence between these two values of 3.6%.

Other EDP exhibit a strange epitaxial situation

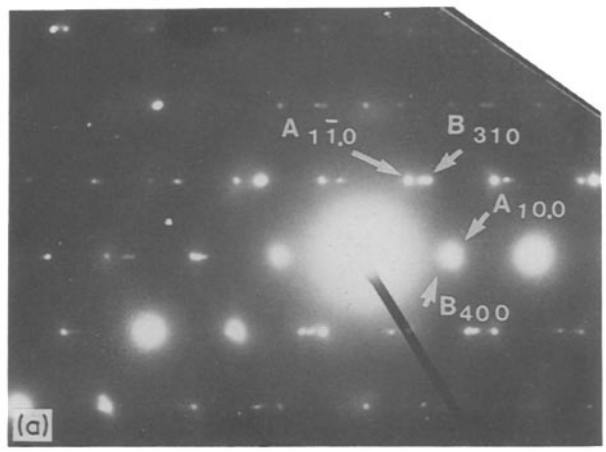

Figure 2 Another well-defined epitaxial correlation between the same structures (see Fig. 1).

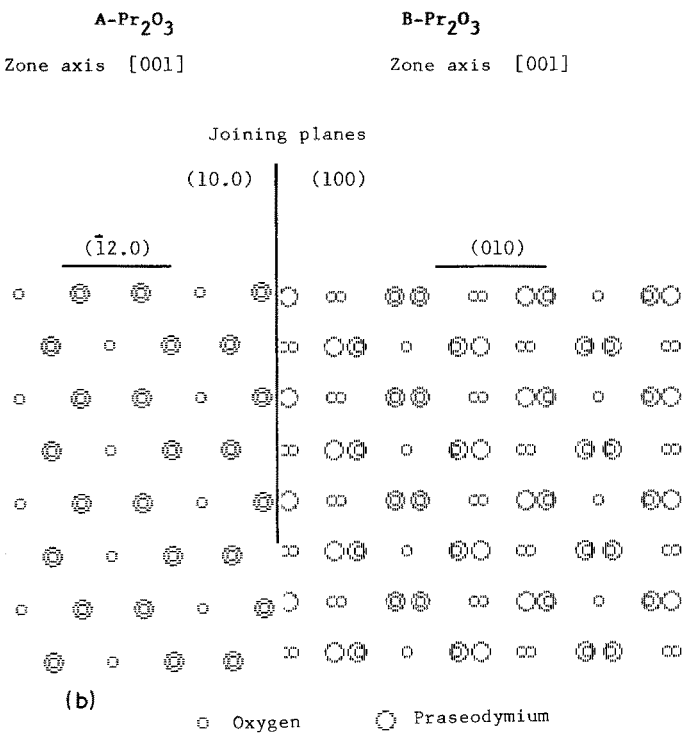

between the A- and B-Pr_2O_3 crystals. These cannot be indexed according to the usual vectorial relationships. Indeed, as shown in Figs 3a and b, the planar indexing of the intense spots can be only done in an asymmetrical manner. For each part of a fictitious plane perpendicular to the central row which passes through the central spot, two different indexes, and therefore two zone axes, are well-defined. In this case the $\langle 0\,1\,0 \rangle$ and $\langle 1\,\bar{3}\,2 \rangle$ axes relative to the B-Pr_2O_3 structure are parallel to the $\langle 0\,0\,1 \rangle$ zone axis of the A-Pr_2O_3 lattice.

It is well known that the B-phase is characterized by numerous twinned domains [21]. One of the possible twins is defined with a twin axis $\langle 1\,\bar{3}\,2 \rangle$ which could play an important role in this pattern. Other patterns are more complex and impossible to index and, at the present time, it is not possible to give a rational explanation.

Figs 4 and 5 exhibit different aspects of two B-Pr_2O_3 crystals. In a general manner crystals such as A- and C-R_2O_3 do not present clearly apparent twins and

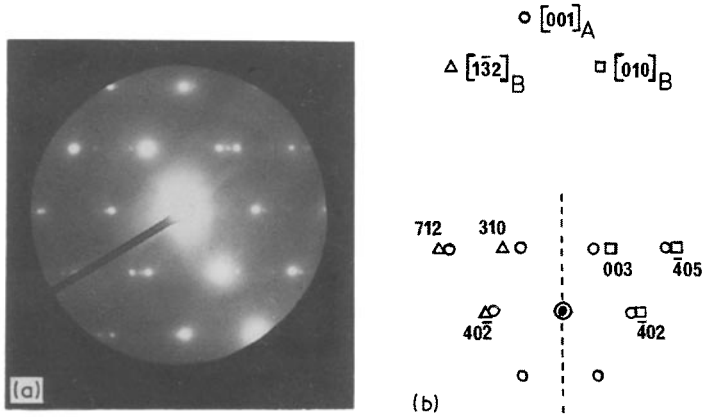

Figure 3 Unusual epitaxial correlation between two A- and B-Pr_2O_3 crystals: each part of the pattern (a) cannot be indexed according to the same zone axis (b).

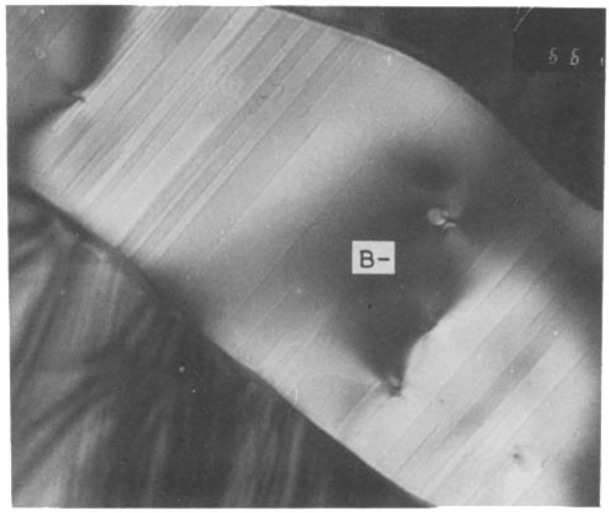

Figure 4 Large B-Pr_2O_3 crystal exhibiting defect network: planar defects or twins.

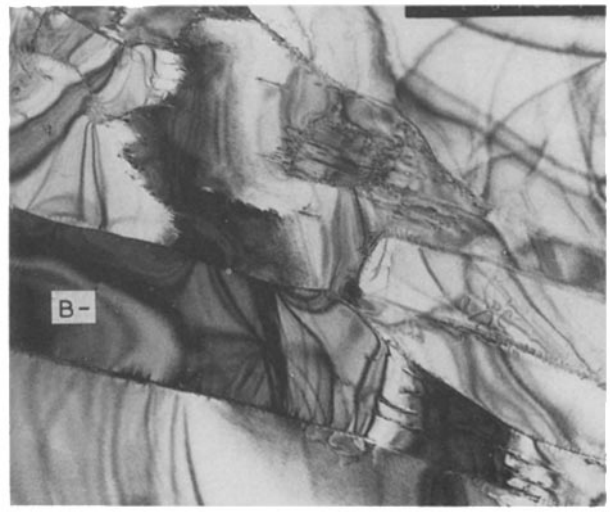

Figure 5 Another B-Pr_2O_3 crystal without defect.

planar defects; they are generally flat or bent with pole figures and extinction contours, but B-Pr_2O_3 crystals are characterized by well-defined twins [21]. In the present case, one crystal is exceptionally characterized by thin planar defects which are suspected to be twins (Fig. 4). In most cases the crystals present a flat appearance (Fig. 5).

3.1.2. A → C epitaxy

Whereas for the A → B epitaxy the crystals appear side by side in the thin film plane, in the A → C case the epitaxy occurs within the thickness of the film (Figs 6a and b). The two zone axes are, respectively, ⟨1 1 1⟩ and ⟨0 0 1⟩. Therefore, the $(1\,1\,1)_C$ and $(0\,0\,.\,1)_A$ planes are superposed. The structure projections

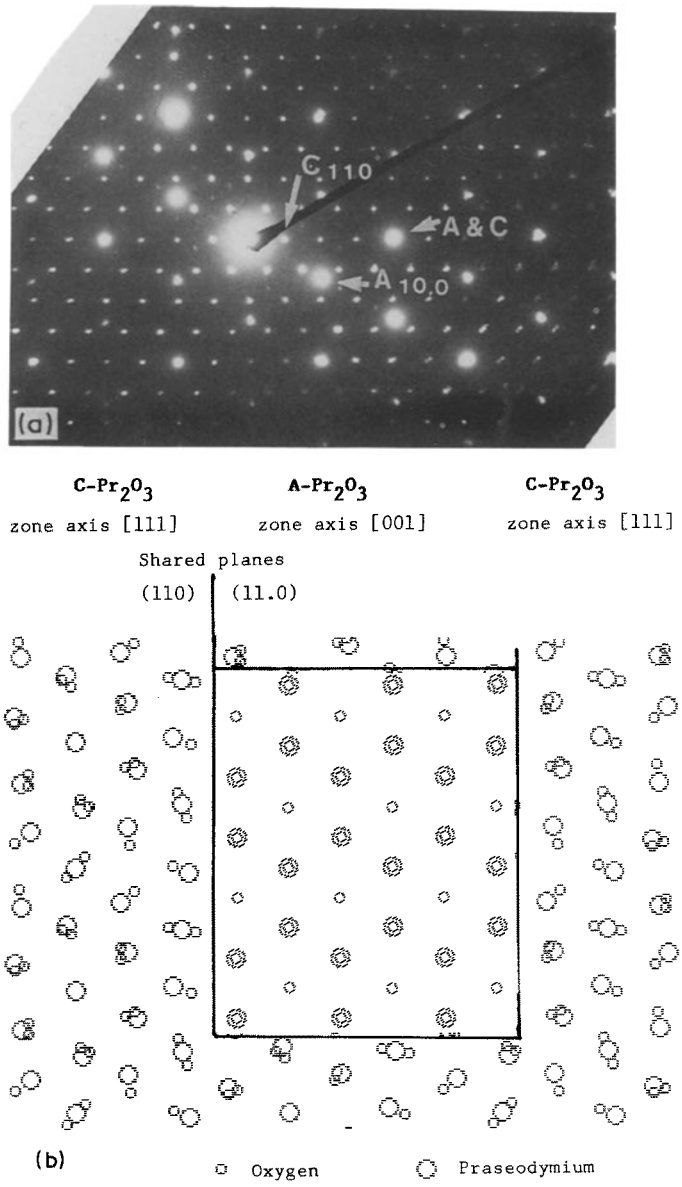

Figure 6 Well-defined epitaxial correlation between A- and C-Pr_2O_3 crystals (see Fig. 1).

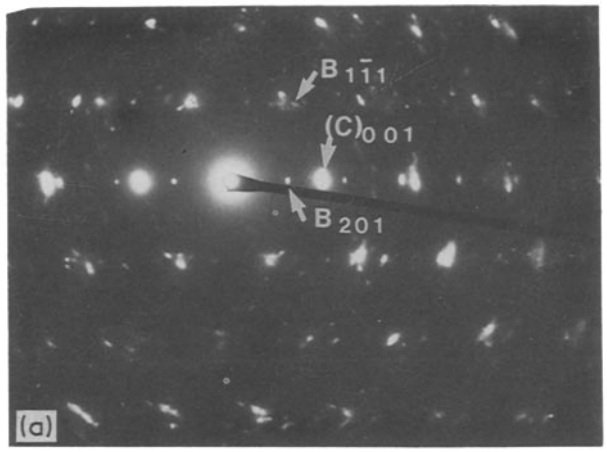

Figure 7 Well-defined epitaxial correlation between TbO_2 and B-Tb_2O_3 crystals (see Fig. 1).

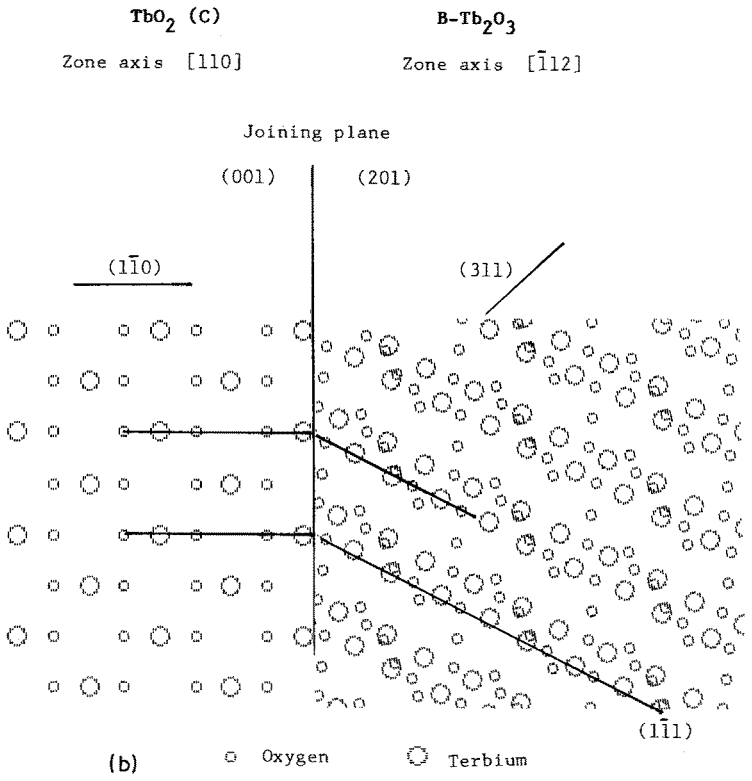

along the zone axes are drawn with the $(1\,1\,0)_C$ plane parallel to the $(1\,1\,.\,0)_A$ one. This leads to the following epitaxial relation:

$$d_{(4\,4\,0)_C} = 0.197\,\text{nm} \quad \text{and}$$

$$d_{(1\,1\,.\,0)_A} = 0.193\,\text{nm}\ (\delta \approx 2\%).$$

One must notice that the corresponding EDP (Fig. 6a) is slightly asymmetric. On the right-hand side the $(4\,4\,0)_C$ and $(1\,1\,.\,0)_A$ diffraction spots seem confused, whereas on the left side they are faintly separated. Classically, as a function of temperature, the C-Pr_2O_3 phase is transformed into the A-Pr_2O_3 structure. The pattern can be an illustration for such a transition, i.e. the rearrangement of the cubic lattice network towards the hexagonal one. Such a crystalline transition was described previously [21].

3.2. Terbium oxides

It is well known that the more stable structure relative to the terbium oxides is the C-Tb_2O_3 phase [1, 2]. However, in thin films, it is very easy to obtain, by electron-beam annealing, the B-Tb_2O_3 structure [21]. In the present case, after water vapour treatment then heating at high temperature, it was also possible to observe the formation of TbO_2.

3.2.1. B-Tb_2O_3 → TbO_2 epitaxy

The first epitaxial situation is for the B-Tb_2O_3 and TbO_2 structures (Figs 7a and b). The two zone axes are, respectively, $\langle \bar{1}\,1\,2 \rangle$ and $\langle \bar{1}\,1\,0 \rangle$. The joining planes are $(2\,0\,1)_B$ and $(0\,0\,1)_{TbO_2}$ as drawn in Fig. 7b. The connecting planes are $(1\,\bar{1}\,1)_B$ and $(1\,\bar{1}\,0)_{TbO_2}$. They are not parallel, because the angle between $(1\,\bar{1}\,1)_B$ and $(2\,0\,1)_B$ is equal to 63.65°. But as the $(1\,\bar{1}\,1)_B$ planes ($d_{1\bar{1}1} = 0.313\,\text{nm}$) intersect the $(2\,0\,1)$ plane with a periodicity equal to 0.350 nm and, as for the TbO_2 structure, the interplanar distance $d_{(1\bar{1}0)} = 0.369\,\text{nm}$, the fit between the two structures is defined within a divergence of about 6%. This fit is less perfect than for A-, B-Pr_2O_3 epitaxy, but one can notice the non-perfect alignment of the different spots on the EDP.

3.2.2. C → B epitaxy

The second epitaxial situation is for the C- and B-Tb_2O_3

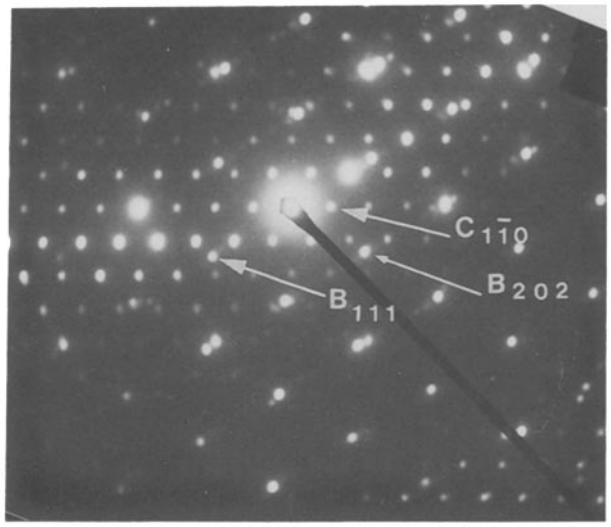

Figure 8 Classical epitaxy between B- and C-Tb_2O_3 structures. The zone axes are $[1\,0\,\bar{1}]_B$ and $[1\,1\,1]_C$, respectively.

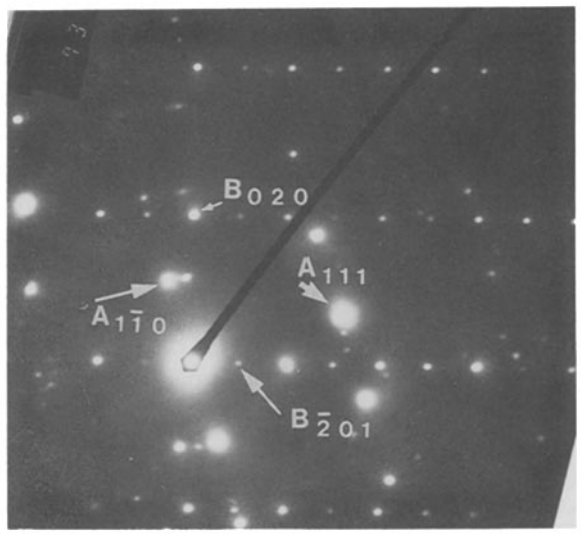

Figure 9 Unusual epitaxial situation between two A- and B-Nd_2O_3 crystals. The two crystals are rotated by 18° compared to each other.

structures (Fig. 8). The pattern is defined by the projection of the two reciprocal lattices, respectively defined by the two zone axes $\langle 1\,1\,1\rangle_C$ and $\langle 1\,0\,\bar{1}\rangle_B$. This implies that the superposed planes are $(1\,1\,1)_C$ and $(2\,0\,1)_B$. These are the basic planes of the well-known OR_4 tetrahedra of the C- and B-R_2O_3 compounds.

3.3. Neodymium oxides

We have previously [21] described in detail the epitaxial situation, sign of a martensitic-type transformation relative to the A- and B-Nd_2O_3 structures. After water-vapour treatment it was possible to obtain a new epitaxial situation due to the existence of stable B-Nd_2O_3 crystals within an A-Nd_2O_3 matrix [22]. The pattern reported in Fig. 9 shows another peculiar case. The two zones axes $\langle 1\,1\,\bar{2}\rangle_A$ and $\langle 1\,0\,2\rangle_B$ are parallel but the two reciprocal lattice projections are rotated by 18° with respect to each other. In this case it was not possible to define an epitaxial relationship between the two crystals.

4. Conclusion

The B-phase in thin films is easily obtained under pulse annealing. Moreover it is stabilized by the water treatment for the ceric group oxides. All this may indicate that the material is submitted during the treatment with the electron beam to some kind of "pressure". It is, in fact, well known that the B-phase is obtained under pressure or shock–stress on bulk materials [23, 24]. Shock reduction has also been applied to Nb_2O_5 [25]. In the present case for praseodymium or terbium we observe in fact an oxidation. We have suggested [14] that the electron-beam impact can be the source of acoustic waves inside thin films. These acoustic waves can couple to, or trigger, low-frequency oxygen modes with large amplitude of vibrations which are suspected to be a basis for "jumps" of oxygen ions into interstitial sites and also to induce phase transitions as shown by a recent lattice dynamics calculation for high T_c superconducting oxides [26]. Optical spectroscopy shows that the rare earth oxides density of phonon states also exhibit sharp phonon modes in the vicinity of 100 cm^{-1} [27]. Water impurities will act as an amplifier of acoustic wave production by enhancing the ablation process, the other source of this type of elastic wave, thermal gradients within the sample surface being the most common one.

References

1. M. FOEX and J. P. TRAVERSE, *Rev. Int. Hautes Temp. Refract.* **3** (1966) 429.
2. *Idem, Bull. Soc. Fran. Miner. Crist.* **89** (1966) 184.
3. P. KNAPPE and L. EYRING, *J. Solid State Chem.* **58** (1985) 312.
4. E. SWEDA, L. EYRING and D. J. SMITH, *Ultramicroscopy* **23** (1987) 443.
5. R. T. TUENGE and L. EYRING, *J. Solid State Chem.* **41** (1982) 75.
6. *Idem, ibid.* **29** (1979) 165.
7. H. A. EICK, L. EYRING, E. SUMMERVILLE and R. T. TUENGE, *ibid.* **42** (1982) 47.
8. E. SUMMERVILLE, R. T. TUENGE and L. EYRING, *ibid.* **24** (1978) 21.
9. Z. C. KANG, D. T. SMITH and L. EYRING, *Surf. Sci.* **175** (1986) 684.
10. C. BOULESTEIX and L. EYRING, *J. Solid State Chem.* **66** (1987) 125.
11. M. GASGNIER, G. SCHIFFMACHER, P. CARO and L. EYRING, *J. Less-Common Metals* **116** (1986) 31.
12. M. GASGNIER, G. SCHIFFMACHER, L. EYRING and P. CARO, *ibid.* **127** (1987) 167.
13. M. GASGNIER, G. SCHIFFMACHER, D. R. SVORONOS and P. CARO, *Inorg. Chem. Acta* **140** (1987) 79.
14. *Idem, J. Microsc. Spectrosc. Electron.* **13** (1988) 13.
15. W. M. SHAFER and R. ROY, *J. Amer. Ceram. Soc.* **42** (1959) 563.
16. V. M. GOLDSCHMIDT, F. ULRICH and T. BARTH, *Geochim. Verteil. Elem., Skrifter Norske Videnskaps-Akad, Oslo, Math. Naturv. Kl.*, **5**, (1925) 5.
17. I. WARSHAW and R. ROY, *J. Phys. Chem.* **65** (1961) 2048.
18. R. S. ROTH and S. J. SCHNEIDER, *J. Res. NBS. A Phys./Chem* **64A** (1960) 309.
19. L. S. PALATNIK, V. E. MARINCHEVA and V. N. TUPIKINA, "Sintez i Svoistva Soedinen Redkozemel Elementov" (Akad. Nauk. SSSR, Oural Nauk Centre, 1982) p. 69.
20. T. NORBY and P. KOFSTAD, in "Reactivity of Solids", edited by P. Barret and L. O. Dufour (Elsevier, Amsterdam, 1985) p. 439.

21. M. GASGNIER, *Phys. Status Solidi (a)* **57** (1980) 11.
22. M. GASGNIER, G. SCHIFFMACHER and P. CARO, *Rev. de Phys. Appl. (Paris)*, **23** (1988) 1341.
23. V. N. GERMAN, A. M. PODURETS and L. A. TARASOVA, *Inorg. Mater.* **18** (1982) 1492.
24. V. A. NERONOV, A. P. VORONIN, M. I. TATARINTSEVA, T. E. MELEKHOVA and V. L. AUSLENDER, *J. Less-Common Metals* **117** (1986) 391.
25. M. KIKUCHI, K. KUSABA, K. FUKUOKA and Y. SYONO, *J. Solid State Chem.* **63** (1986) 386.
26. P. BRUESCH and W. BUHRER, *Z. Phys. B Condensed Matter* **70** (1988) 1.
27. P. CARO, O. K. MOUNE, E. ANTIC-FIDANCEV and M. LEMAITRE-BLAISE, *J. Less-Common Metals* **112** (1985) 153.

Received 3 May
and accepted 9 September 1988